Research Square

Preprints are preliminary reports that have not undergone peer review.
They should not be considered conclusive, used to inform clinical practice,
or referenced by the media as validated information.

Probabilistic assessment of uncertainty of carbon capture and storage for achieving Paris-Aligned goals

Luis Felipe Sivolella

luis.sivolella@ppe.ufrj.br

Centre for Energy and Environmental Economics (Cenergia), Energy Planning Program (PPE), Coppe, Universidade Federal do Rio de https://orcid.org/0009-0001-2889-1664

Luiz Bernardo Baptista

Universidade Federal do Rio de Janeiro https://orcid.org/0000-0002-7016-1796

Gerd Angelkorte

UFRJ https://orcid.org/0000-0003-0385-4565

Pedro Rochedo

Khalifa University https://orcid.org/0000-0001-5151-0893

Alexandre Szklo

Universidade Federal do Rio de Janeiro https://orcid.org/0000-0002-7101-1810

Roberto Schaeffer

Universidade Federal do Rio de Janeiro https://orcid.org/0000-0002-3709-7323

Article

Keywords:

Posted Date: March 26th, 2026

DOI: https://doi.org/10.21203/rs.3.rs-9159548/v1

License: This work is licensed under a Creative Commons Attribution 4.0 International License.
Read Full License

Additional Declarations: There is **NO** Competing Interest.

Probabilistic assessment of uncertainty of carbon capture and storage for achieving Paris-Aligned goals

Luis Felipe Sivolella*
luis.sivolella@ppe.ufrj.br
https://orcid.org/0009-0001-2889-1664
Centre for Energy and Environmental Economics (Cenergia), Energy Planning Program (PPE), Coppe, Universidade Federal do Rio de Janeiro / Rio de Janeiro - Brazil

Luiz Bernardo Baptista
luizbernardo@ppe.ufrj.br
https://orcid.org/0000-0002-7016-1796
Centre for Energy and Environmental Economics (Cenergia), Energy Planning Program (PPE), Coppe, Universidade Federal do Rio de Janeiro / Rio de Janeiro – Brazil

Gerd Angelkorte
angelkorte@ppe.ufrj.br
https://orcid.org/0000-0003-0385-4565
Centre for Energy and Environmental Economics (Cenergia), Energy Planning Program (PPE), Coppe, Universidade Federal do Rio de Janeiro / Rio de Janeiro – Brazil

Pedro Rochedo
pedro.rochedo@ku.ac.ae
https://orcid.org/0000-0001-5151-0893
Research and Innovation Center on CO_2 and Hydrogen (RICH Center) and Management Science and Engineering Department, Khalifa University / Abu Dhabi – UAE

Alexandre Szklo
szklo@ppe.ufrj.br
https://orcid.org/0000-0002-7101-1810
Centre for Energy and Environmental Economics (Cenergia), Energy Planning Program (PPE), Coppe, Universidade Federal do Rio de Janeiro / Rio de Janeiro - Brazil

Roberto Schaeffer
roberto@ppe.ufrj.br
https://orcid.org/0000-0002-3709-7323
Centre for Energy and Environmental Economics (Cenergia), Energy Planning Program (PPE), Coppe, Universidade Federal do Rio de Janeiro / Rio de Janeiro - Brazil

Abstract

The Paris Agreement's ambition to limit global warming to well below 2.0ºC with an aspirational 1.5ºC goal relies on the rapid, large-scale, and sustained deployment carbon dioxide removal (CDR) and carbon capture and storage (CCS) technologies. IPCC's Sixth Assessment Report outlines different pathways through deterministic runs of integrated assessment models (IAMs), whose findings led to technically feasible scenarios with abundant storage utilization. However, real-world institutional and market barriers and storage uncertainty imply that the window of flexible mitigation policies is closing. To assess this, we employ a sampling-based stochastic framework comprising 2,500 global IAM scenarios, allowing statistical inference of energy, land use and emissions outcomes. Our results for 1.5ºC and 2.0ºC goals show a large-scale reliance on land-based CDR to bridge the gap and compensate for residual emissions. In addition, the scale of geological storage frequently exceeds "prudent planetary limits" across critical regions producing a concerning trend for beyond 2100.

Introduction

Limiting global warming to 1.5°C or 2.0°C above preindustrial levels requires rapid emission reductions with strict management of the remaining global carbon budget[1,2]. However, current emission trajectories remain misaligned with these goals[3–5], increasing the likelihood of overshoot and reinforcing the need to address residual emissions from hard-to-abate sectors[6]. Therefore, mitigation strategies increasingly consider not only conventional decarbonization measures - energy efficiency, electrification, and low-carbon sources - but also carbon capture and storage (CCS) linked to energy and industrial sectors and traditional and novel carbon dioxide removal (CDR)[7–9] options used as a complementary component of long-term climate stabilization strategy. However, most of these technologies lack an extensive deployment record at the scales implied and with projected levels that often exceed historical rates of large-scale energy infrastructure expansion. In addition, significant questions persist concerning biophysical and geological limits, including sustainability of biomass, and permanence risks, and the effective capacity of geological CO_2 storage reservoirs [10,11].

The uncertainty of carbon capture and removal technologies

Achieving climate change mitigation policy goals is increasingly tied to the large-scale deployment of fossil CCS, bioenergy with carbon capture and storage (BECCS), afforestation/reforestation (A/R), biochar, enhanced weathering (EW) and direct air carbon capture (DAC)[12,13] (Supplementary Table 1). This reliance introduces significant uncertainty into decarbonization strategies.

These uncertainties are not only technical, but also economic, infrastructural, geological, and social in nature, making long-term estimates, such as those from IAMs results, and real-world policy planning more difficult[14,15]. In the CCS case, infrastructure for CO_2 transport and storage remains a major bottleneck, as the cost of building and operating extensive CO_2 pipeline networks varies widely across regions and assumptions, depending heavily on economies of scale and geographic factors[16]. Designing such infrastructure under uncertainty - particularly regarding the location and capacity of future capture sources - raises the risk of stranded assets

and underutilized systems[17]. Geological uncertainty adds another layer of complexity, since local injectivity, sealing integrity, and public acceptance remain poorly characterized in many regions[18], although technical potential estimates for geological CO_2 storage are abundant[19]. Even small variations in techno-economic parameters such as capture efficiency, storage rates, and learning curves can have outsized impacts on the viability of CCS in climate mitigation scenarios. CDR technologies are subject to even greater uncertainty regarding scale, cost, and permanence. Achieving gigaton-scale CO_2 removal through technologies such as A/R, biochar and BECCS entails massive land use. Specifically, for BECCS, the biomass supply chain and biofuel production rely on integration with carbon storage infrastructures. Each stage of these combined systems - from cultivation to long-term storage - is associated with significant technical, ecological, and socio-political uncertainties. IAMs frequently over-rely on these options, assuming large-scale removals by mid-century despite unclear feasibility[8,20].

IAMs under uncertainty

IAMs serve as the primary analytical tool for planning and evaluating climate emergency mitigation strategies[21,22]. Through the definition of specific scenarios, an IAM enables the identification of possible pathways for energy, socioeconomic, and environmental planning, or alternatively, for assessing the consequences of the current polices and measures taken[23]. A substantial challenge of this approach is the uncertainty in the quantification of model parameters, including the pace of technological innovation and diffusion, market dynamics, and socioeconomic trends[24–26].

Recent efforts were made to incorporate uncertainty explicitly within IAM frameworks[27–31]. However, comprehensive uncertainty propagation remains computationally demanding, particularly for large-scale optimizing models with high sectoral and regional resolution. As result, uncertainty is often explored indirectly through multi-model ensembles[32,33], rather than incorporated directly into an IAM. That approach, while broadening the scenario space and providing insight for evaluating and planning, does not constitute a fully probabilistic treatment: models differ in assumptions, calibration, and structure, limiting the internal coherence of aggregated results.

To incorporate uncertainty in a global IAM, we employ a multi-scenario framework that perform statistical inference over the solution space of energy, land-use, and emission variables using a sampling-based stochastic approach with the COFFEE model[34] (Supplementary Methods). We generate two ensembles of 1,250 scenarios with carbon budgets goals consistent with 1.5ºC and 2.0ºC temperature increase limits and introduce CCS uncertainty through the IPCC AR6[35] C2 and C3 ensembles data, extracting the CCS maximum deployment capacity and starting year of deployment, thereby capturing a broad spectrum of mitigation strategies consistent with stringent climate goals (Supplementary Methods) - a modeling choice that enables the construction of scenarios that reflect the wide range of plausible CCS deployment pathways and their interactions with complementary and substitute CDR technologies and other strategies. For this CCS capacity constraint, a five-year deployment delay from the original dataset was implemented to account for the time elapsed since the C2 and C3 ensemble results were produced, along with a regional participation index that balances infrastructure readiness with economic scale. Uncertainty in the regional carbon storage limits was also introduced, using the three levels of capacity defined by Gidden et al.[19] spatially explicit study that considers the existing infrastructure, the harm prevention and risk avoidance scenario, and the technical potential, which were adapted to the COFFEE's 18 native regions (Supplementary Methods).

Results

Emission, capture and removal

Delayed mitigation actions intensify the mitigation efforts required in the latter half of the century. By mid-century, the ensemble exhibits (Fig. 1a) substantial residual emissions of 6.96 (6.31; 7.69)[1]* $GtCO_2$ for the 1.5ºC ensemble - this is consistent with the interquartile range (IQR) of the C2 ensemble[35] - and 21.75 (21.29; 22.20) $GtCO_2$ for the 2.0ºC target - beyond the P95 of the C3 ensemble[35]. The persistence of positive emissions in 2050 requires compensatory scale-up of CDR technologies to satisfy the remaining carbon budget of those scenarios. By 2100, the 1.5ºC ensemble is forced into substantial net-negative territory, reaching a median emission level of -17.10 (-17.96; -16.00) $GtCO_2$. This requirement is 50% larger than that of the 2.0ºC ensemble, -11.00 (11.71; -10.02) $GtCO_2$, which also trends toward deeper negative emissions. Both results sit in the lower quartile (P5-P25) range of the C2 and C3 pathways, respectively[35].

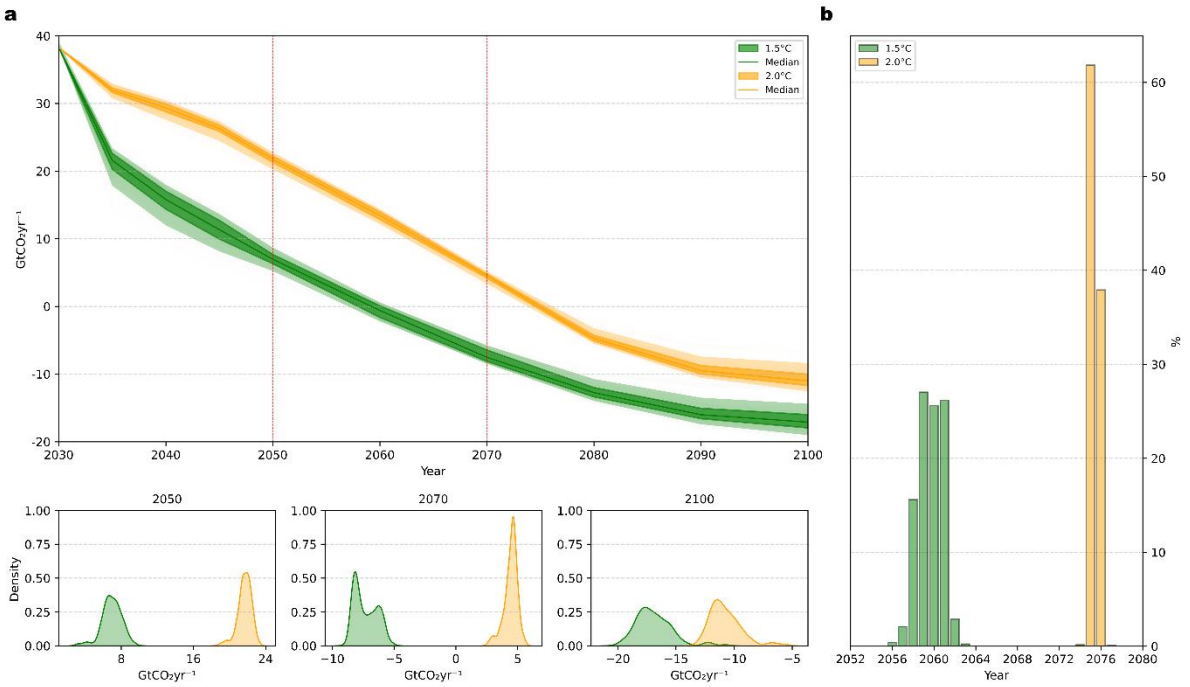


Figure 1 | CO_2 emission trajectory and CO_2 net-zero years distribution. a, Time-series of global net CO_2 emissions in $GtCO_2yr^{-1}$ for 1.5ºC (green) and 2.0ºC (yellow) ensembles (1,250 scenarios per ensemble). Solid central lines represent each ensemble median; darker shaded areas denote the central 50% quantile range (P25-P75), and lighter shaded areas denote central 90% quantile range (P5-P95) bottom subpanels display the kernel density estimation (KDE) for emissions in the 2050, 2070, and 2100 milestones with lines and shaded areas in density curves representing the 100% quantile. **b**, Probability distribution of global net-zero CO_2 years across for 1.5ºC (green) and 2.0ºC (yellow) ensembles (1,250 scenarios per ensemble). Bar graph of frequency (%) of the year of the crossing point of global CO_2 emissions into negative territory.

Regarding the timing of global net-zero CO_2 emissions, the 1.5ºC ensemble displays a tight distribution clustered in the late 2050s and early 2060s. Specifically, net-zero CO_2 emissions are concentrated between 2057 and 2061, which accounts for nearly 95% of all scenarios (Fig. 1b). For the 2.0ºC goal, the distribution is shifted toward the end of the century and is clustered

[1]* Hereafter, values are reported as median (Q1; Q3), where Q1 and Q3 correspond to the 25th (P25) and 75th (P75) percentiles, respectively, defining the interquartile range (IQR), which encompasses the central 50% of the distribution.

between the years 2075 and 2076 in more than 99% of all scenarios. These results are consistent with the interquartile range (IQR) of IPCC AR6 C2 and C3 ensemble, respectively[35].

The mid-of-century mitigation under the 1.5ºC goal (Fig. 2a) is primarily met through land-based measures, with A/R, biochar and soil carbon management (SCM) providing a median of 3.92 (3.92; 3.93) $GtCO_2yr^{-1}$. This 2050 deployment requires growth rate for A/R nears the upper limits of 13 $Mhayr^{-1}$ for this ensemble[36]. At this milestone, BECCS also begins to scale, contributing 0.85 (0.67; 1.11) $GtCO_2yr^{-1}$, while other novel CDR technologies such as EW and DAC remain negligible.

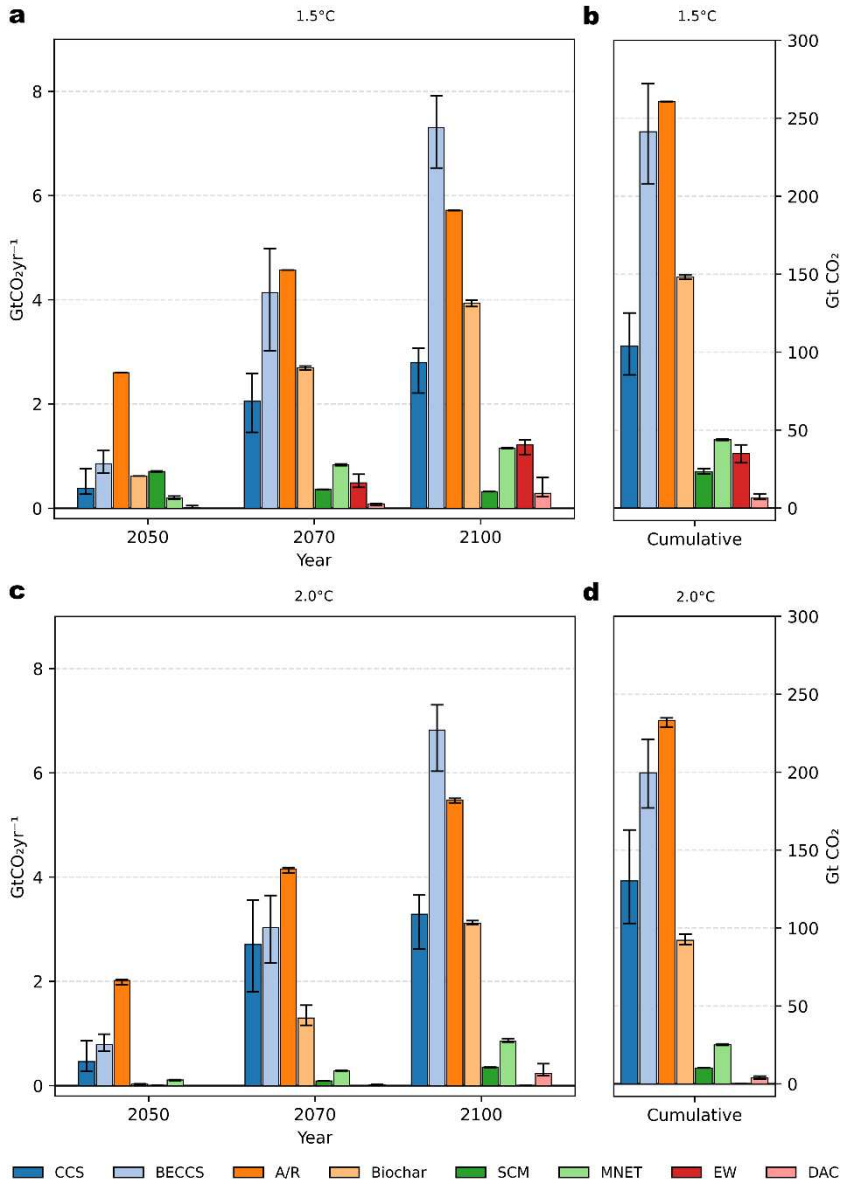


Figure 2 | Portfolio of carbon sequestration and cumulative carbon sequestration. a, c, Time-series of annual sequestration in $GtCO_2yr^{-1}$ for the 1.5ºC and 2.0ºC ensembles (1,250 scenarios per ensemble) at years 2050, 2070, and 2100. **b**, **d**, Right-hand panels depict the cumulative sequestration in $GtCO_2$ for each technology over the 2026-2100 period for the 1.5ºC and 2.0ºC ensembles (1,250 scenarios per ensemble). **a**, **b**, **c**, **d**, Technologies include fossil and industrial carbon capture and storage (CCS), bioenergy with carbon capture and storage (BECCS), afforestation/reforestation (A/R), biochar, soil carbon management (SCM), materials (MNET), enhanced weathering (EW), and direct air capture (DAC). Bars represent the ensemble median; whiskers denote the central 50% quantile range (P25-P75). Results are shown for the (**a**, **b**) 1.5ºC and (**c, d**) 2.0ºC ensembles.

The need for a higher effort in this mitigation window becomes evident in the rapid scaling of these technologies toward the mid of the century. In 2070, A/R (Fig. 2a) achieves median of 4.57 (4.57; 4.57) $GtCO_2yr^{-1}$, biochar reaches 2.69 (2.65; 2.73) and BECCS reaches 4.14 (3.03; 4.99) $GtCO_2yr^{-1}$. By 2100, the model relies on of its entire carbon sequestration portfolio. A/R reaches its saturation level of 5.72 (5.71; 5.73) $GtCO_2yr^{-1}$, while BECCS scales to 7.30 (6.53; 7.92) $GtCO_2yr^{-1}$. Notably, other novel CDR technologies, which were not as relevant in 2050, provide, comparatively, small sequestration contributions by 2100, with MNET, EW and biochar contributing a median of 1.15 (1.14; 1.16), 1.21 (1.03; 1.31) and 3.93 (3.87; 3.99) $GtCO_2yr^{-1}$ respectively and DAC deployment emerging at 0.28 (0.22; 0.59) $GtCO_2yr^{-1}$. This suggests that the model prioritizes more cost-efficient land-intensive measures (A/R and biochar) to meet the mitigation obligations.

In the 2.0ºC ensemble (Fig. 2c), mid-century reliance on land-based removals is substantially lower, with A/R providing a median of 2.01 (1.93; 2.03) $GtCO_2yr^{-1}$. BECCS also is representative with 0.78 (0.66; 0.99) $GtCO_2yr^{-1}$. However, as the century progresses, both pathways converge toward high sequestration levels to compensate for early-action delays. In 2070 A/R achieves 4.15 (4.08; 4.18) $GtCO_2yr^{-1}$ and BECCS reaches 3.03 (2.35; 3.65) $GtCO_2yr^{-1}$. By 2100, the 2.0ºC ensemble reaches a median A/R of 5.47 (5.42; 5.51) $GtCO_2yr^{-1}$, and BECCS 6.82 (6.03; 7.31) $GtCO_2yr^{-1}$. The novel CDR technologies have smaller contributions in the 2.0ºC ensemble in the sequestration portfolio, reaching in 2100, 0.85 (0.83; 0.90) $GtCO_2yr^{-1}$ with MNET and 3.12 (3.09; 3.17) $GtCO_2yr^{-1}$ with biochar, and with a negligible contribution from EW.

For fossil-based CCS, the 2.0ºC ensemble (Fig. 2c) consistently requires higher deployment volumes and more aggressive growth rates than the 1.5ºC ensemble (Fig. 2a) in the long term. The CCS median for the 2.0ºC ensemble (Fig. 2c) ascend to 0.46 (0.28; 0.86) $GtCO_2yr^{-1}$ in 2050 and climbs to 3.29 (2.62; 3.65) $GtCO_2yr^{-1}$ by 2100. Notably, this exceeds the 1.5ºC ensemble's (Fig. 2a) mid-century value of 0.38 (0.27; 0.76) $GtCO2yr^{-1}$and 2.79 (2.21; 3.07) $GtCO_2yr^{-1}$ in 2100.

Cumulative sequestration data highlight the reliance in land-based CDR technologies. For the 1.5ºC pathways (Fig. 2b), the predominant cumulative sink reaches a median of 260.63 (260.57; 260.72) $GtCO_2$ for A/R, 241.29 (207.99; 272.17) $GtCO_2$ for BECCS and 148.12 (146.80; 149.37) $GtCO_2$ for biochar. In comparison, the 2.0ºC ensemble (Fig. 2d) requires 233.13 (228.99; 234.72) $GtCO_2$ for A/R, 199.62 (177.01; 221.08) $GtCO_2$ for BECCS and 92.10 (89.29; 96.05) $GtCO_2$ for biochar. Relatively less significant, the novel CDR technologies MNET, EW and DAC sum up to a median of 85.44 (80.12; 90.88) $GtCO_2$ for 1.5ºC ensemble (Fig. 2b), and 29.05 (28.14; 29.81) $GtCO_2$ for 2.0ºC ensemble (Fig. 2d). The marginal role of these high-cost technologies suggests they function as portfolio balancers only when land-based measures approach saturation. The fossil-based CCS account for approximately 103.75 (85.35; 125.12) $GtCO_2$ for 1.5ºC ensemble (Fig. 2b) and a higher 130.29 (102.92; 162.89) $GtCO_2$ for the 2.0ºC ensemble (Fig. 2d), reflecting a scenario where the more lenient carbon budget permits a slower phase-out of fossil-based energy systems if paired with carbon capture and combined with BECCS shows the total demand on geologic storage is significant.

Median of carbon sequestration technology for both 1.5ºC and 2.0ºC ensembles are in the respective C2 and C3 envelopes (Supplementary Figs. 1a, b), and for most results within the P5-P95 range.

Sectoral net emissions

The sectoral net emissions across the 1.5°C and 2.0°C ensembles (Figs. 3a, b) show that the energy and agriculture, forestry, and other land use (AFOLU) sectors are key for phasing-out carbon emissions, when compared with the industrial sector and other capture and removal technologies.

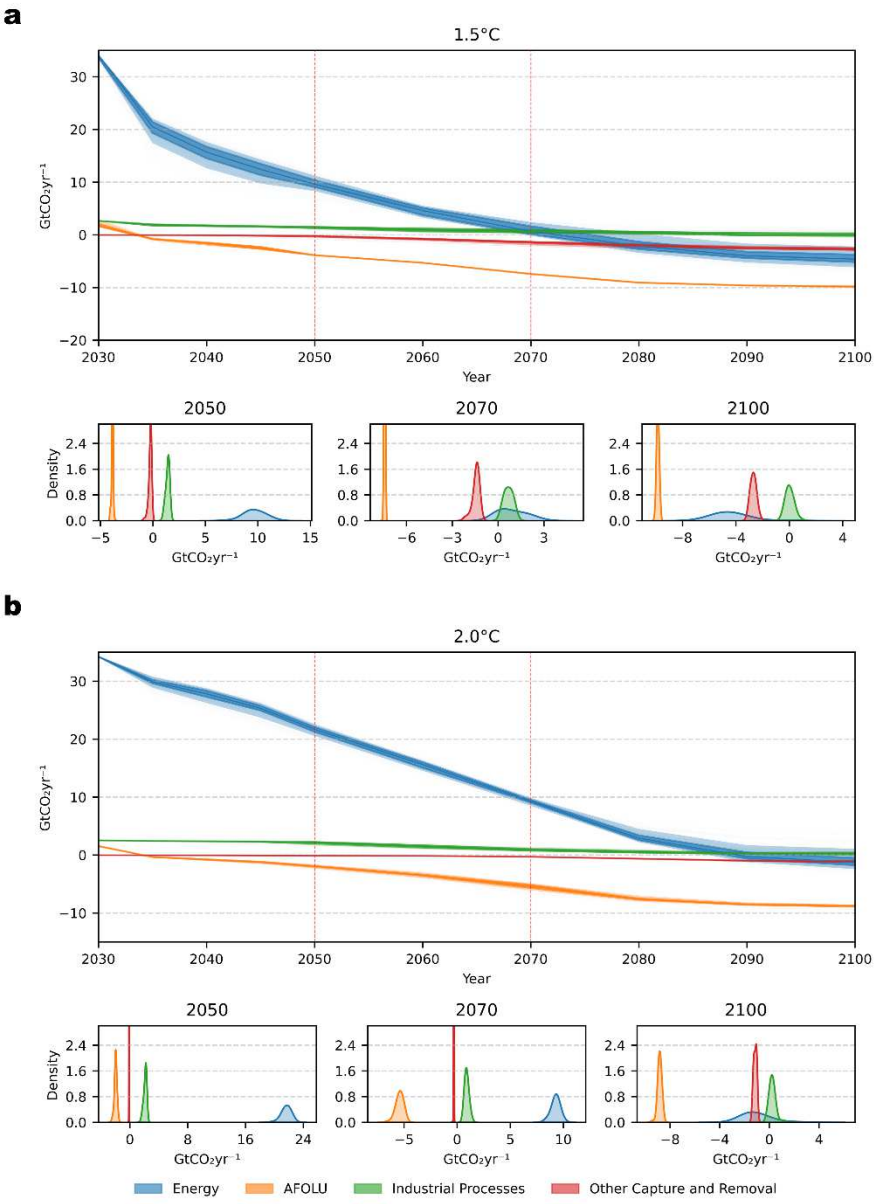


Figure 3 | Sectoral net emissions. a, **b**, Time-series of global sectoral net emissions**,** capture and removal for 1.5°C and 2.0°C ensembles (1,250 scenarios per ensemble). Sectoral net emissions, categorized into energy, agriculture, forestry, and other land use (AFOLU), industrial processes, and other capture and removals - representing non-sectorial capture and removal direct air carbon capture (DAC), enhanced weathering (EW), materials (MNET). Darker shaded areas denote the central 50% quantile range (P25-P75), and lighter shaded areas denote central 90% quantile range (P5-P95); bottom subpanels display the kernel density estimation (KDE) for emissions in the 2050, 2070, and 2100 milestones with lines and shaded areas in density curves representing the 100% quantile. Results are shown for the (**a**) 1.5ºC and (**b**) 2.0ºC ensembles.

The sectoral distribution of net emissions in the 1.5ºC ensemble (Fig. 3a) reinforces a rapid transition toward net-negative CO_2 emissions, with strong reliance on land-based removals and a deep decarbonization of the energy system. By 2050, AFOLU already provides substantial net-negative emissions of -3.85 (-3.87; -3.85) $GtCO_2yr^{-1}$, offsetting still-positive emissions from the energy sector at 9.61 (9.06; 10.39) $GtCO_2yr^{-1}$ and industrial processes at 1.46 (1.30; 1.52) $GtCO_2yr^{-1}$, while other capture and removal technologies contribute -0.21 (-0.28; -0.18) $GtCO_2yr^{-1}$. This balance shifts markedly by 2100, when the system becomes net-negative across most sectors: AFOLU removals deepen to -9.85 (-9,91; -9,79) $GtCO_2yr^{-1}$, energy net emissions turn strongly negative at -4.61 (-5.19; -3.74) $GtCO_2yr^{-1}$, and other capture and removal reaches -2.69 (-2.86; -2.55) $GtCO_2yr^{-1}$. Industrial emissions are largely neutralized, with a median of -0.01 (-0.2; 0.2) $GtCO_2yr^{-1}$, indicating near-complete abatement. This trajectory highlights an early and sustained mitigation effort, where negative emissions scale rapidly and dominate the long-term prospect.

In contrast, the 2.0ºC ensemble (Fig. 3b) exhibits a more gradual transition, with higher residual emissions in mid-century and a delayed shift toward net-negative outcomes. In 2050, energy emissions remain substantially higher at 21.70 (21.27; 22.08) $GtCO_2yr^{-1}$ - more than double those in the 1.5ºC case - while AFOLU removals are comparatively limited at -1.98 (-2.01; -1.89) $GtCO_2yr^{-1}$, and other capture and removal contributes only -0.11 (-0.12; -0.10) $GtCO_2yr^{-1}$. Industrial emissions are also higher at 2.18 (2.01; 2.27) $GtCO_2yr^{-1}$. By 2100, the system does move toward net-negative emissions, but less uniformly: AFOLU reaches -8.83 (-8.91; -8.73) $GtCO_2yr^{-1}$ and energy becomes moderately negative at -1.28 (-1.78; -0.50) $GtCO_2yr^{-1}$, while other capture and removal contributes -1.12 (-1.25; -1.03) $GtCO_2yr^{-1}$. However, industrial emissions remain positive at 0.21 (0.10; 0.37) $GtCO_2yr^{-1}$. Overall, compared to the 1.5ºC ensemble (Fig. 3a), the 2.0ºC ensemble (Fig. 3b) delays mitigation in the energy sector and relies less intensively on AFOLU and other capture and removal, resulting in a later and weaker transition to net-negative emissions by the end of the century.

Primary energy, electrification and hydrogen

As expected, the projection of global primary energy in the 1.5ºC and 2.0ºC ensembles (Figs. 4a, b) shows a transformation characterized by the phase-down of fossil fuels and a transition towards renewable sources. In the 1.5ºC pathway (Fig. 4a), median fossil source consumption drops from 496.86 (492.22; 498.24) $EJyr^{-1}$ in 2030 to 163.09 (159.99; 166.38) $EJyr^{-1}$ by 2100. To compensate, biomass emerges as the main energy sources, scaling from median of 70.53 (69.79; 71.02) $EJyr^{-1}$ and in 2030 to a median of 539.04 (528.87; 549.98) $EJyr^{-1}$ by 2100. Similarly, non-biomass renewables exhibit significant growth, from 64.84 (62.66; 68.93) $EJyr^{-1}$ in 2030, reaching 403.96 (395.91; 411.54) $EJyr^{-1}$ by the century's end, while nuclear energy provides a stable, albeit smaller, contribution, increasing from 15.44 (14.41; 15.51) in 2030 to 49.74 (49.56; 49.94) $EJyr^{-1}$ by the end of the century.

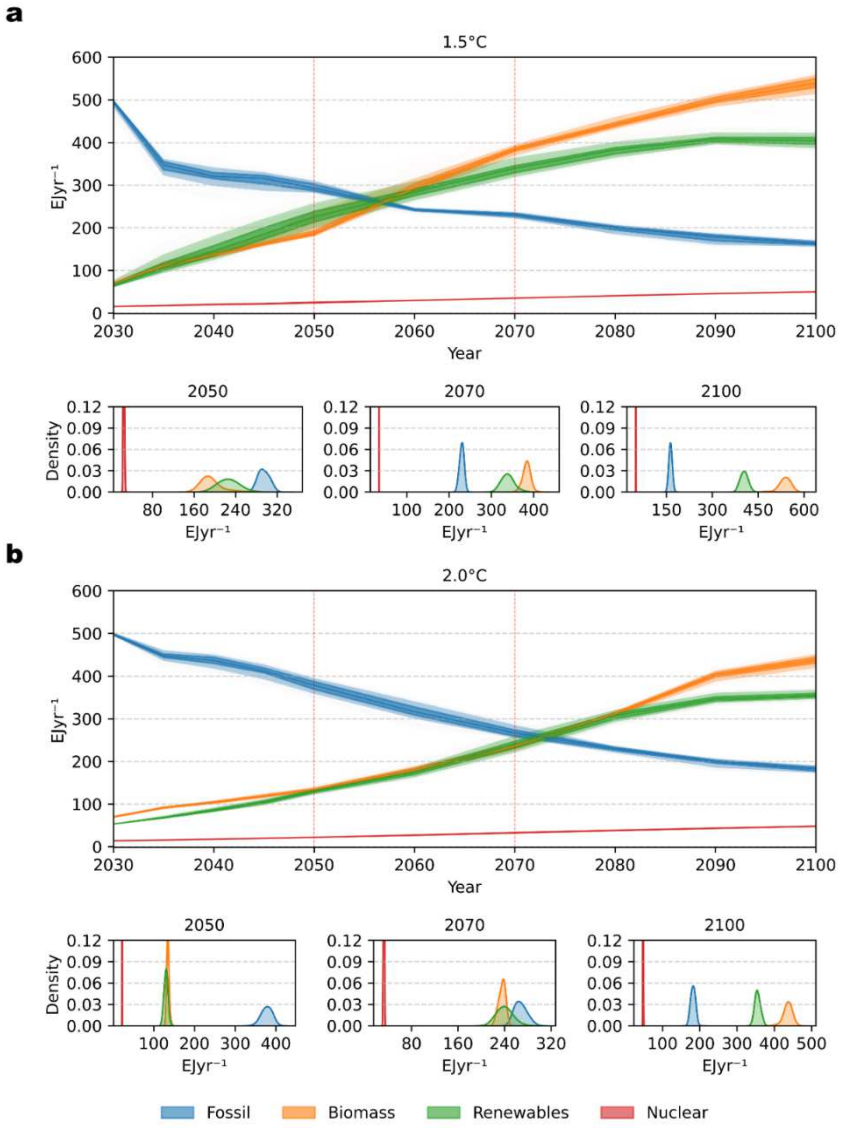


Figure 4 | Primary energy. a, **b**, Time-series of global primary energy sources in $EJyr^{-1}$ for 1.5ºC and 2.0ºC ensembles (1,250 scenarios per ensemble). Primary energy categorized into fossils, biomass, renewables (representing non-biomass renewable sources), and nuclear. Darker shaded areas denote the central 50% quantile range (P25-P75), and lighter shaded areas denote central 90% quantile range (P5-P95); bottom subpanels display the kernel density estimation (KDE) for primary energy in 2030, 2050, 2070, and 2100 milestones with lines and shaded areas in density curves representing the 100% quantile. Results are shown for the (**a**) 1.5ºC and (**b**) 2.0ºC ensembles.

The 2.0ºC ensemble (Fig. 4b) follows a similar but more gradual shift. Fossil fuel consumption remains higher in the medium term, reaching median of 182.13 (177.79; 186.12) $EJyr^{-1}$ by 2100. Consequently, the reliance on biomass is less extreme than in the 1.5ºC case, with a requirement of 437.30 (431.00; 443.92) $EJyr^{-1}$ at the end of the century. Simultaneously, non-biomass renewables in the 2.0ºC pathway grow to 354.44 (350.78; 359.37) $EJyr^{-1}$, while nuclear energy provides a stable contribution, increasing to 48.00 (47.44; 48.24) $EJyr^{-1}$.

Both ensembles exhibit similar behavior where the biomass and non-biomass renewables pathways converge into the mid of the century and diverge at the end of the century in favor of biofuels. As expected, the 2.0ºC ensemble (Fig. 4b) has a larger flexibility in the energy transition allowing for a softer landing of the fossil with both biomass and non-biomass renewables having a very similar role until the very end of the century, in which the use of

biomass provide further negative emission relive. On the other hand, the 1.5ºC ensemble (Fig. 4a) relies on a higher non-biomass renewable output and is pushed toward higher biomass and lower fossil configurations.

Median of primary energy sources for both 1.5ºC and 2.0ºC ensembles are in the respective C2 and C3 envelopes (Supplementary Figs. 2a, b), with the notable exception of the biomass, which in C2/C3 envelopes by the end of the century, which may stem from specific IAM protocols regarding biomass supply constraints[49,50].

The share indicators of the global energy quantify a rapid transition, where the relative composition of primary energy shifts from fossil-dominated to a biomass and renewable-centric structure. In the 1.5ºC ensemble, the fossil share (Fig. 5a) undergoes a compression, falling from a median of 76.78 (76.00; 77.08) % in 2030 to just 14.15 (13.85; 14.43) % by 2100. Inversely, the biomass share (Fig. 5b) expands from 10.90 (10.79; 10.97) % in 2030 to 46.69 (46.18; 47.10) % by 2100. This indicates that almost half of global primary energy would be derived from biomass sources. The scaling of renewables sources further defines this shift, with wind (Fig. 5c) and solar PV shares (Fig. 5d) in the 1.5ºC ensemble reaching medians of 14.88 (14.57; 15.10) % and 17.85 (17.68; 18.14) % respectively by 2100.

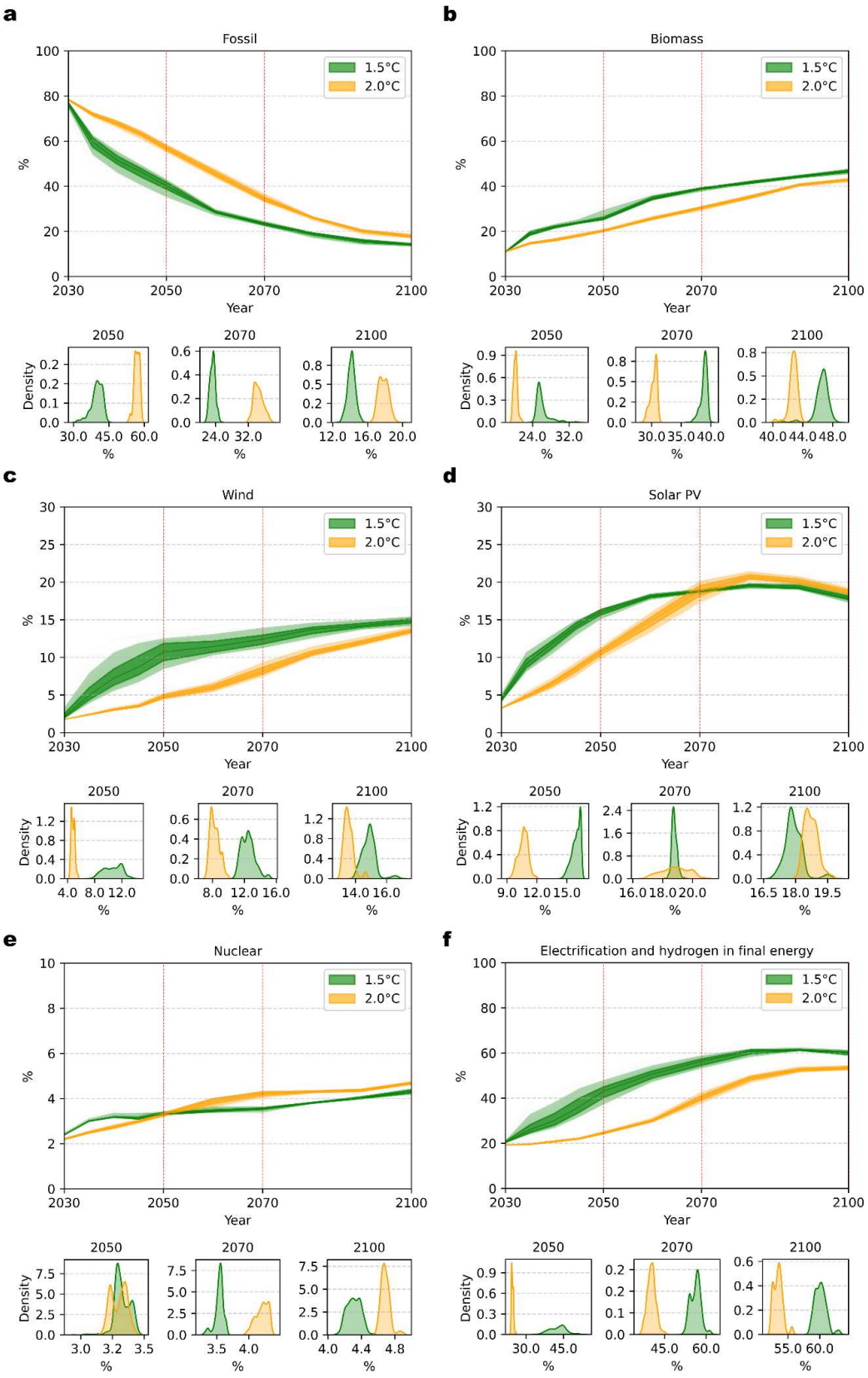


Figure 5 | Shares of primary energy sources and share of electrification and hydrogen in final energy. a-f, Time-series of share in primary energy sources and share electrification and hydrogen in final energy for 1.5ºC and 2.0ºC ensembles (1,250 scenarios per ensemble). Share (%) of the global energy system for 1.5ºC (green) and 2.0ºC (yellow) ensembles, including (**a**) fossil, (**b**) biomass, (**c**) wind, and (**d**) solar PV, and (**e**) nuclear in primary

energy, alongside the (**f**) electrification and hydrogen share in final energy. Darker shaded areas denote the central 50% quantile range (P25-P75), and lighter shaded areas denote central 90% quantile range (P5-P95); bottom subpanels display the kernel density estimation (KDE) for emissions in the 2050, 2070, and 2100 milestones with lines and shaded areas in density curves representing the 100% quantile.

In the 2.0ºC ensemble, the transition is slightly decelerated but follows a similar trajectory, with fossils (Fig. 5a) still holding 17.79 (17.37; 18.23) % of the mix by century's end. Biomass (Fig. 5b) reaches 42.78 (42.26; 43.11) %, wind (Fig. 5c) and solar PV (Fig. 5d) reaches similar end-century results (compared to 1.5ºC ensemble) of 13.50 (13.33; 13.72) % and 18.69 (18.47; 18.94) % although with different trajectories which in the less ambitious climate goal with lower but steady growth rate in the early to mid-century.

The energy transition occurs for both ensembles through a massive surge in electrification and hydrogen (Fig. 5f) consumption, which rises in the from 20.50 (20.35; 20.78) % in 2030 to 60.08 (59.41; 60.66) % of final energy by 2100. The electrification and hydrogen share have the largest difference between the ensembles diverging between mid-century to and the end-century which reaches for the 2.0ºC ensemble median of 53.45 (52.86; 53.86) % for 2100. Lastly, for both ensembles, nuclear (Fig. 5e) share has a similar trajectory reaching 4.31 (4.25; 4.37) % and 4.68 (4.65; 4.72) % respectively in 2100.

Discussion

Land use implications of CDR deployment

The deployment of nature-based solutions (NBS) in the 1.5°C and 2.0°C ensembles reveal a profound reconfiguration of global land systems throughout the century. In both scenarios, land allocation to CDR options expands modestly until mid-century and accelerates sharply thereafter, particularly under the 1.5°C pathway. The stricter mitigation constraint translates into earlier scaling and substantially larger cumulative land requirements by 2100.

Under 1.5°C, the afforestation/reforestation (A/R) process increases progressively after 2030 (Fig. 6a), with strong regional concentrations in China, Russia, Sub-Saharan Africa, and Latin America, achieving 895.50 (894.20; 896.40) Mha in 2100. In contrast, the 2.0°C pathway exhibits a more gradual expansion of A/R (Fig. 6a), with lower medians and narrower IQRs, reflecting greater flexibility in mitigation options and reduced pressure for large-scale land-based removals, accumulating 824.03 (799.75; 833.27) Mha in 2100. It is important to highlight that, in the 1.5°C scenario, there is a saturation of the A/R development potential throughout most of the analyzed period (Fig. 6b), approaching the model's maximum potential of around 900 Mha (Fig. 6a). Furthermore, although the 2.0°C scenario shows a lower cumulative A/R, this divergence occurs mainly in the first years of the analysis (Fig. 6b). After 2060, however, both scenarios show similar behavior, reaching the maximum of about 12 Mha of A/R per year (Fig. 6b).

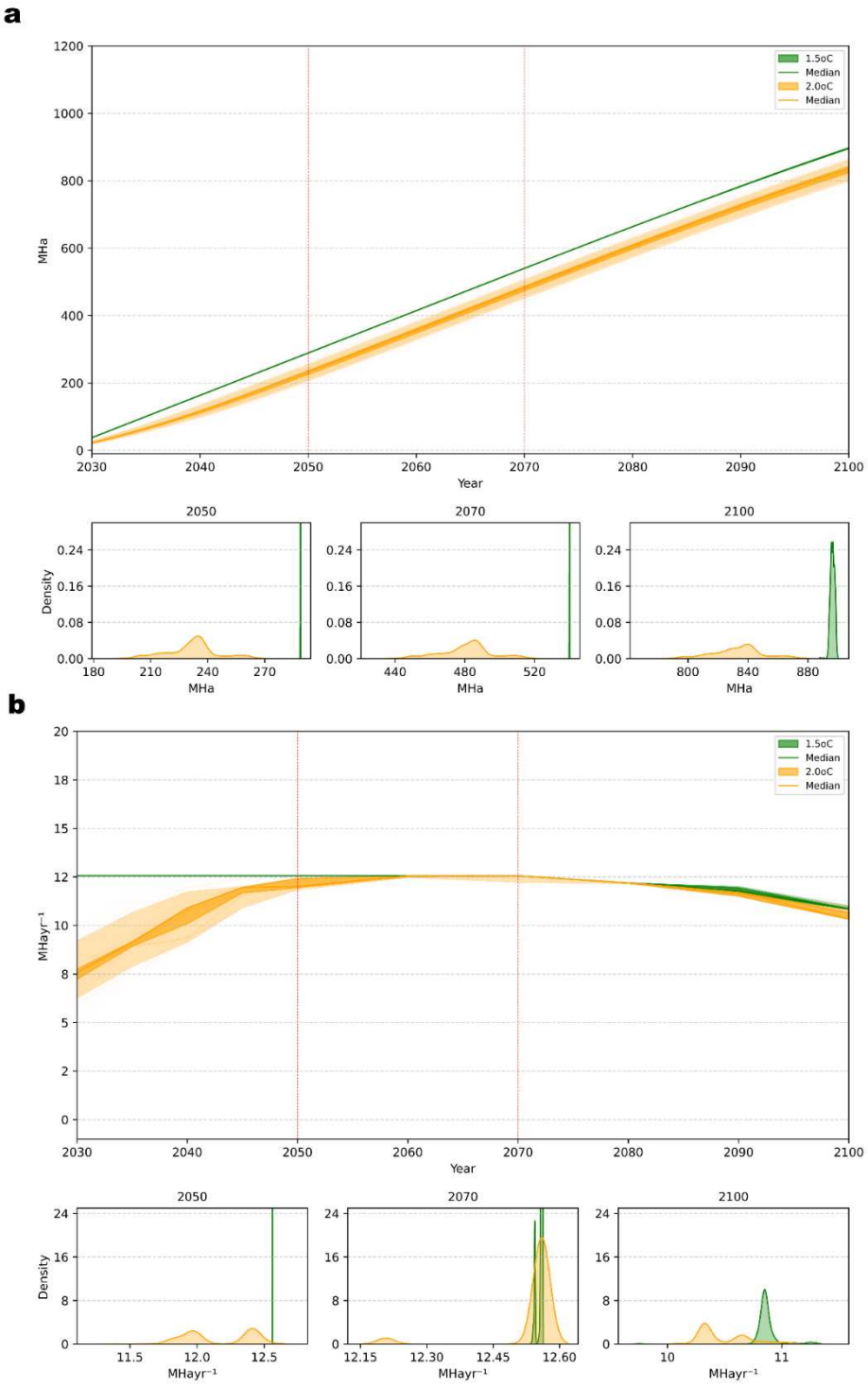


Figure 6 | Afforestation/reforestation cumulative and annual land increase area. a, Time-series of cumulative land area of Afforestation/reforestation (A/R) in MHa for the 1.5ºC and 2.0ºC ensembles (1,250 scenarios per ensemble) at years 2050, 2070, and 2100. **b**, Time-series of annual land area increase of A/R in $MHayr^{-1}$ for the 1.5ºC and 2.0ºC ensembles (1,250 scenarios per ensemble). **a, b,** Solid central lines represent each ensemble median; darker shaded areas denote the central 50% quantile range (P25-P75), and lighter shaded areas denote central 90% quantile range (P5-P95) bottom subpanels display the kernel density estimation (KDE) for 2050, 2070, and 2100 milestones with lines and shaded areas in density curves representing the 100% quantile.

EW and biochar show even greater divergence between ensembles. In the 1.5°C, EW scales rapidly after 2060, with India, Sub-Saharan Africa, and parts of Latin America emerging as

major deployment regions, reaching values above 150 Mha of area produced with EW as early as 2080 and a maximum potential of 202.66 (172.10; 217.66) by 2100. Biochar presents an important cumulative land transformation, particularly in Africa, China, and India, where agricultural systems are substantially reconfigured to integrate biomass production and soil carbon enhancement, achieving 496.58 (488.80; 504.45) Mha in 2100. At 2.0°C, biochar expands at a more moderate rate, and EW becomes significant only after 2080, but with comparatively limited penetration until 2100, mainly for EW: 393.50 (389.65; 399.60) Mha for biochar and 300.00 (284.38; 423.41) kha for EW.

The expansion of land-based CDR also raises important concerns regarding competition with food production. Large-scale biochar deployment requires sustained biomass supply chains that may compete directly or indirectly with cropland, pasture, or feed production. Similarly, extensive restoration efforts may constrain agricultural expansion or intensification in regions with growing food demand. These interactions suggest that stringent mitigation pathways, particularly the 1.5°C scenario, could intensify land-use trade-offs unless accompanied by substantial gains in agricultural productivity, dietary transitions, or reductions in food loss and waste.

An important caveat is that the projections presented here do not explicitly account for land disturbances such as wildfires, pests, or extreme climate-driven ecosystem losses. As seen by Griscom et al.[37] and Streck et al.,[18] in restoration-based pathways (active reforestation and natural restoration), carbon permanence depends on ecosystem stability over decadal timescales. Increased wildfire frequency and intensity under climate change could compromise stored carbon stocks, reduce net removal efficiency, and potentially require additional land to compensate for reversal risks. Therefore, the effective land requirement associated with NBS deployment may be underestimated in disturbance-prone regions.

Implications of geological carbon storage and its 'prudent planetary limits'

The analysis of onshore and offshore regional geological storage utilization (Figs. 7a, b) reveals discrepancies between projected capture and storage requirements and sustainable 'prudent planetary limits', as proposed by Gidden et al.[19]. The authors present spatially defined planetary limits (socially and environmentally constrained) and the geological technical potentials (theoretical maximum capacity). When comparing our study results with data provided by Gidden et al., it shows that India (IN) and Europe (EU) and Eastern Europe (XE), are operating in a state of significant geological over-leverage on both onshore (Fig. 7a) of offshore (Fig. 7b) geological storage. Japan (JP) and Korea (KR) also display a high-profile risk, which is worsened by the lack of feasible onshore capacity. China (CH) exhibits a comparatively less mismatch between projected storage demand and sustainable geological capacity, however, capacity constraints may emerge as a concern in the post-2100 period.

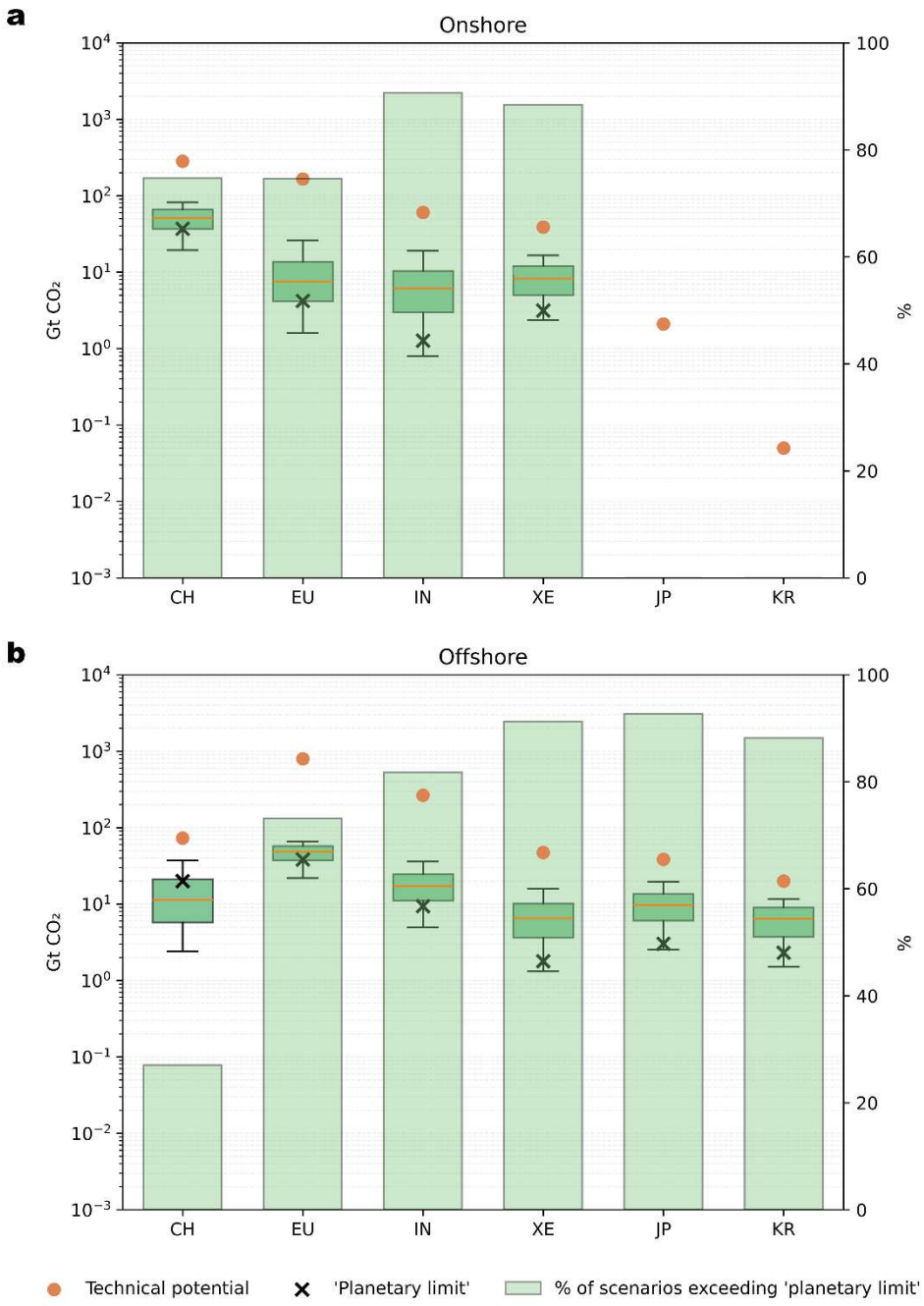


Figure 7 | Cumulative onshore and offshore geological carbon storage reached in 2100, technical potential, and "prudent planetary limit" across critical regions. a, **b**, Boxplots (median, box P25-P75, and whiskers P5-P95) represent the distribution of cumulative geological carbon storage for the 1.5ºC ensemble across six critical regions: China (CH), Europe (EU), India (IN), Eastern Europe (XE), Japan (JP), and Korea (KR). The left y-axis (logarithmic scale) denotes cumulative storage in $GtCO_2$. Geological carbon storage technical potentials are indicated by red dots, while regional 'prudent planetary limit' for sustainable storage are marked with an "×". JP and KR have onshore 'prudent planetary limit' of 0 $GtCO_2$ thus are not represented in the logarithmic scale. The lighted shaded green bars and with corresponding right y-axis indicate the percentage of scenarios that exceed the designated 'prudent planetary limit'.

In CH, the onshore sector (Fig. 7a) displays a high risk of over-utilization, with a median sequestration of 50.79 (36.92; 65.54) $GtCO_2$ surpassing the planetary limit of 37.04 $GtCO_2$ in 74.7% of scenarios, indicating a pronounced vulnerability to long-term capacity exceedance. In contrast, the offshore (Fig. 7b) sector remains largely within sustainable bounds: the

planetary limit is estimated at 20.02 $GtCO_2$, while the median utilization reaches 11.33 (5.73; 21.08) $GtCO_2$, with only 27.0% of scenarios exceeding the planetary threshold. EU exhibits a comparable higher risk profile with both areas with over-utilization, particularly onshore (Fig. 7a), where the median utilization 7.58 (4.18; 13.68) $GtCO_2$ is double the planetary limit 4.21 $GtCO_2$, with over 74.6% of scenarios failing to remain within sustainable constraints. In the EU offshore sector (Fig. 7b), the utilization median reaches 48.75 (37.4; 57.17) $GtCO_2$ which exceeds 38.25 $GtCO_2$ in 73.1% of the scenarios

In IN, the discrepancy is most acute in the onshore sector (Fig. 7a), where the median utilization in the 1.5ºC ensemble of 6.18 (2.93; 10.39) $GtCO_2$ is nearly five times higher than the planetary limit of 1.27 $GtCO_2$, with 90.6% of scenarios breaching this threshold. In the offshore sector (Fig. 7b) the median in IN is 17.12 (11.14; 24.41) $GtCO_2$, which is almost twice as much the planetary limit of 9.38 $GtCO_2$, with 81.8% of scenarios beyond the planetary limit. For XE, the median sequestration the offshore sector (Fig. 7b) reaches median of 6.51 (3.61; 10.11) $GtCO_2$ and it is more than triple the planetary limit of 1.79 GtCO2, resulting in 91.3% of scenarios exceeding the prudent boundary and with onshore (Fig. 7a) median of 8.24 (4.98; 11.96) $GtCO_2$ and a planetary limit of 3.15 $GtCO_2$ with 88.4% of scenarios beyond the planetary limit. KR and JP offshore sector (Fig. 7b) has similar over-utilization of carbon storage in our results: KR with median of 6.45 (3.69; 9.08) $GtCO_2$ for a planetary limit of 2.31 $GtCO_2$ and 88.2% of scenarios beyond planetary limit and JP with median of 9.76 (6.04; 13.69) $GtCO_2$ for a planetary limit of 3.02 $GtCO_2$ and 92.7% of scenarios beyond planetary limit.

The sampling-based stochastic framework

Although, this study provides an initial exercise in systematic quantification of uncertainty within a unified model-framework and employing a global IAM, it opens avenues for future research in many topics regarding parametric uncertainty. Stochastic disturbance of cost, efficiency, capacity, construction time, and other parameters, as well as model constraints can be employed to evaluate uncertainty in IAM results. Complementing ensemble-based analysis, a stochastic framework enables a more rigorous identification of critical pathways, system resilience, and technological constraints, strengthening the basis for climate policy under deep uncertainty. In this study, the identification of a narrow mitigation pathway for land-based measures, as well as the assessment of the geological storage “prudent planetary limit,” relies on this approach.

Ultimately, our model results reinforce the view that the window of flexible mitigation policies is really closing and that a robust mitigation strategy requires the deployment of a broad range of CDR options. Furthermore, the 1.5ºC and 2.0ºC ensembles exhibit a strong reliance on A/R - approaching saturation-level - as well as BECCS, together with a substantial transition toward bioenergy. Moreover, the results show the prospect of over-utilization of geological storage that may push beyond ‘prudent planetary limits’ in critical regions by 2100, potentially compromising the long-term viability of this technological pathway.

Methods

Global IAM COFFEE

The COFFEE (Computable Framework For Energy and the Environment) model is a deterministic IAM formulated for intertemporal optimization of energy and land use systems

on a global scale under partial economic equilibrium with an objective of minimization of total system costs while meeting energy and food service demands and being subject to a set of constraints. COFFEE is built upon the MESSAGE linear programming platform developed by the International Institute for Applied System Analysis (IIASA). A comprehensive description of the model structure, demand assumptions, technology portfolio and model region breakdown, can be found in Zanon-Zotin, et al.[38], and Müller-Casseres, et al.[39].

This study employs two ensembles of scenarios with different carbon budgets of the COFFEE model within the sampling-based stochastic framework.

Sampling-based stochastic framework

The sampling-based stochastic framework adopted in this study (Fig. 8) has three main components: Uncertainty Analysis (UA)[40], Monte Carlo Method (MCM)[41], and Statistical Analysis (SA)[42].

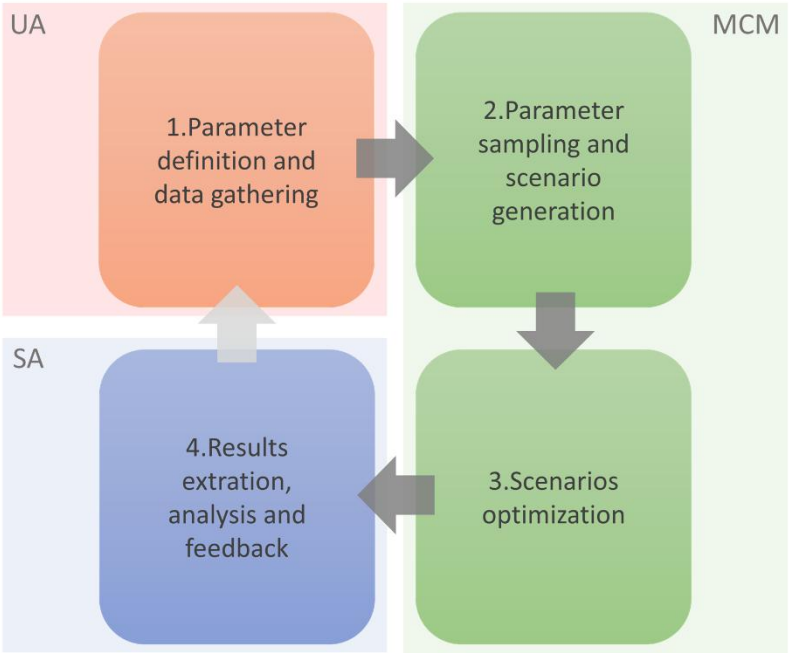


Figure 8 | Sampling-based stochastic framework workflow. The workflow integrates Uncertainty Analysis (UA), Monte Carlo Method (MCM), and Statistical Analysis (SA) in four individual steps.

Consistent with the structure presented in Figure 8, the individual steps are detailed below.

1. Parameter definition and data gathering: The parameters of the IAM are assessed to quantify their impact on the model set of variables and constraints of importance for the analysis. The parameters are classified by the effect in the results and then selected according to its significance. Considering the parameter selection defined previously, data from current development stages, projected learning curves, specialist's insight and results or constraints from IAM ensembles are assembled and processed as probability distributions - probability density function (PDF), probability mass function (PMF) or kernel density estimation (KDE) - to be used as the selected parameters for the model.

2. Parameter sampling and scenario generation: Parameter instances are generated based on the probability distributions defined during the UA. Model instances with parametric sampling are created.

3. Scenario optimization: A high-performance computing (HPC) system receives the ensemble of parameterized models to perform large-scale multi-instance optimization.

4. Result extraction, analysis and feedback: The raw output data from the optimizations are collected and processed to derive probability distributions for key variables of interest. The output data are subjected to both descriptive and inferential statistical analysis. Data from statistical techniques provide feedback for the UA, making it possible for their refining.

Uncertainty characterization in this study

The probabilistic characterization of uncertainty in this study is achieved through the application of the MCM within selected model parameters of the IAM COFFEE, implemented using Latin hypercube sampling (LHS)[43]. This approach provides a framework for reproducing stochastic system behavior and exploring uncertainty space through the implementation of multiple deterministic model scenarios. The aggregated ensemble of outcomes statistically converges toward the underlying probability distribution of the system response, enabling a consistent quantification of uncertainty propagation, and the estimation of expected values and uncertainty ranges, under the influence of the uncertainty introduction assumptions.

The uncertainty introduction for this study considers two critical dimensions of CCS uncertainty in our models: the CCS capacity deployment and the geological carbon storage limit. For this purpose, we created probability distribution functions that relies on the IPCC AR6 scenario database[35] using the C2 and C3 ensembles as proxy of expert elicitation surveys, which considers general assumptions about starting point and maximum potential of the technology. We adapted the aforementioned data to consider a five-year delay, input of the historical capacity data and a participation index to define the regional deployment that considers industrial GDP and exiting oil and gas pipeline infrastructure. This approach considers regional differences in capacity to deploy large-scale CCS infrastructure. As for the geological carbon storage, we generated a regional triangular distribution function that considers the three levels of storage capacity defined in Gidden et al.[19] spatially explicit study: the potential in basins with installed oil & gas infrastructure, the sensible limit that account for harm prevention and risk avoidance, and the geological technical potential.

Supplementary Figures 3-5 present comparisons between the parameters used to characterize CCS uncertainty and their realizations across the ensembles.

We generate two ensembles of carbon budget targets for temperature increases of 1.5ºC, and 2.0ºC above pre-industrial levels by 2100 considering socioeconomic assumptions that are consistent with shared socioeconomic pathway (SSP) framework[44] and defined as SSP2 scenario. For each CO2 budget, 1,250 scenarios were generated, providing a statistically meaningful representation of the uncertainty space. The ensemble size was determined to provide, a priori, a 5% error (of the standard deviation) at a 90% confidence level considering adherence to the central limit theory (CLT). The ensembles' overall assumptions are consolidated in Table 1.

Table 1 | Ensemble overall definitions

Ensemble	Socioeconomics	Carbon budget ($GtCO_2$)	Sample size
1.5ºC	SSP2	400	1250
2.0ºC	SSP2	1150	1250

Note: AR6 WGI carbon budget from 2010 to 2100 consistent with likelihood scale of 66-100% probability ("Likely"). Source: adapted from IPCC[45].

Uncertainty introduction

Global CCS limits

The global time-series constraint of CCS capacity in our ensembles is modeled using a logistic function, consistent with the technological diffusion for large-scale energy infrastructure and specifically CCS deployment[4]. The sequestration capacity curve P(t), by the logistic function is defined as:

$$P(t) = \frac{L}{1 + e^{-k(t-t_0)}}$$

where L is the maximum sequestration capacity, k is the logistic growth rate, and t_0 is the midpoint of the transition. The growth rate k was bounded with a symmetrical triangular distribution between 0.05 and 0.25, defined considering the range found in the majority (97%) of the scenarios in the C2 and C3 ensembles.

To define the CCS limit modeling, we extracted two key parameters from the "Carbon Sequestration|CCS" variable of the C2 and C3 ensembles: the onset year, defined as the year sequestration exceeds a 250 Mt $CO2yr^{-1}$ threshold, where we introduce a five-year delay, and the maximum sequestration value of the time-series. These values serve in the scenario as the boundary conditions for transport of sequestered carbon to geological storage. In this case, this constraint also encompassed DAC, working as a total limit for all carbon capture and storage technologies. The validation of the generated parameters against IPCC AR6 dataset is shown in Figure 9.

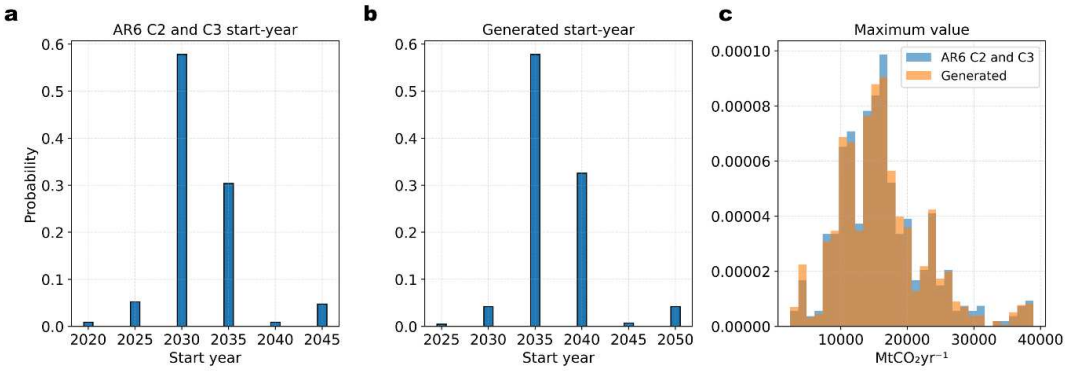


Figure 9 | Parameters validation against IPCC AR6 dataset. Probabilistic distributions of CCS parameters of the ensembles. **a**, Probability mass function (PMF) of the starting years for CCS deployment (threshold > 250 Mt $CO2yr^{-1}$) derived from the IPCC AR6 C2 and C3 scenario database. **b**, PMF of the starting years generated for the ensembles, reflecting the enforced five-year mitigation delay. **c**, Comparative distribution of the maximum annual sequestration capacity. Empirical values from the IPCC AR6 C2 and C3 (blue) are contrasted with the generated ensemble capacities (orange), demonstrating that the generated curves preserve the statistical characteristics of the AR6 data.

Regional CCS limits

The regional projected allocation of the global carbon sequestration limit is determined by a index that represents the region's proportional share of the global total, calculated as the arithmetic mean of the regional density of oil and gas pipelines - defined as total pipeline length (km)[46] per unit of land area (Ha) - and the 2020 industry value added in current USD[47].

$$I_{reg} = 0.5\left(\frac{D_{reg}}{D_{total}} + \frac{V_{reg}}{V_{total}}\right)$$

In this formulation, D_{reg} denotes the density of oil and gas pipelines per unit of regional area, while V_{reg} represents the industry value added in 2020. The denominators, D_{total} and V_{total} are the global aggregates of these respective variables' reflection each region's relative contribution to the global capacity.

To account for regional uncertainty in deployment and policy, the final share is sampled from a triangular distribution. The index defines the central tendency (mode) of this distribution, while the minimum and maximum parameters establish the probabilistic bounds for the region's actual participation in global sequestration. Regions with participation indices ~5% or above are categorized as high-capacity, utilizing tighter probabilistic bounds (25% around the mode), whereas those below 5% are classified as low-capacity with higher variability (50%). This framework allows the creation of scenarios in a range of deployment outcomes across the 18 regions, as shown in Table 2.

Table 2 | Regional CCS limit participation definition

Region	Share Index	Capacity category	Min factor	Mode factor	Max factor
Africa (AF)	0.0223	Low	0.5	1	1.5
Australia & NZ (AU)	0.0121	Low	0.5	1	1.5
Brazil (BR)	0.0091	Low	0.5	1	1.5
Canada (CA)	0.0267	Low	0.5	1	1.5
Canada (CD)	0.0252	Low	0.5	1	1.5
Caspian Region (CP)	0.0258	Low	0.5	1	1.5
China (CH)	0.1617	High	0.75	1	1.25
European Union (EU)	0.1448	High	0.75	1	1.25
India (IN)	0.0547	High	0.75	1	1.25
Japan (JP)	0.0364	Low	0.5	1	1.5
Middle East (ME)	0.0797	High	0.75	1	1.25
Rest of Asia (RA)	0.0313	Low	0.5	1	1.5
Russia (RU)	0.0405	Low	0.5	1	1.5
South Africa (SF)	0.0055	Low	0.5	1	1.5
South America (SM)	0.0298	Low	0.5	1	1.5
South Korea (KR)	0.0498	High	0.75	1	1.25
United States (US)	0.2010	High	0.75	1	1.25
Eastern Europe (XE)	0.0436	Low	0.5	1	1.5

Note: Adapted from World Bank[47] and Global Energy Monitor[46]

Table 3 provides the regional CCS capacity baselines from 2010 through the 2025, sourced from the IEA CCUS database[48]. These empirical values, in Mt CO2, serve as the historical constraints for the sequestration limits applied to the ensembles.

Table 3 | Regional historical CCS data

Region	2010	2015	2020	2025 (Projected)
Africa (AF)	0	0	0	0.001
Australia & NZ (AU)	0	0	1.6	3.3
Brazil (BR)	0	10.6	10.6	10.6
Canada (CA)	0	0	0	0
Canada (CD)	0	1.1	1.1	1.1
China (CH)	0	0.1	0.7	5
Caspian Region (CP)	0	0	0	0
European Union (EU)	1.86	1.86	1.86	1.9
India (IN)	0	0	0	0
Japan (JP)	0	0	0	0
South Korea (KR)	0	0	0	0
Middle East (ME)	0	0.8	3.7	8
Rest of Asia (RA)	0	0	0	3.3
Russia (RU)	0	0	0	0
South Africa (SF)	0	0	0	0
South America (SM)	0	0	0	0
United States (US)	16.16	19.32	21.22	23.525
Eastern Europe (XE)	0	0	0	0

Note: Values in Mt CO2. Adapted from IEA CCUS database[48]

Geological carbon storage

The geological carbon storage constraint applied in this ensemble is derived from the regional assessment of Gidden et al.[19], adapted to the 18 regions of the model. Onshore and offshore storage potentials are treated separately to preserve differences in resource characterization, infrastructure maturity, and accessibility. For each region, storage availability is parameterized by using triangular distributions to reflect structured uncertainty in technically recoverable capacity.

The minimum, mode, and maximum of onshore (Table 4) and offshore (Table 5) parameters define the triangular distributions which is the upper bound of availability of geological carbon storage that can be accessed within the ensemble scenarios. The parameterization follows the three constraints framework: the minimum corresponds to storage volumes associated with existing oil and gas infrastructure; the mode represents the “prudent” planetary storage limit; and the maximum reflects the full technical potential based on geological assessments. Together, these bounds provide a representation of storage uncertainty across regions while maintaining alignment with established geophysical research. Because the maximum is substantially higher than the mode, the distribution is heavily skewed to the maximum, leading most scenarios to utilize capacities above the defined prudent limit. This, in turn, allows us to

evaluate the frequency of threshold exceedance, while also assessing feasibility concerns in individual scenarios where lower values are drawn.

Table 4 | Onshore regional triangular distribution parameters

Region	Minimum	Mode	Maximum
Africa (AF)	38.75	293.32	1,206.44
Australia & NZ (AU)	52.36	70.51	313.08
Brazil (BR)	33.22	52.9	231.5
Canada (CA)	8.38	11.9	89.38
China (CH)	3.53	37.04	283.18
Caspian Region (CP)	4.79	50.67	413.89
European Union (EU)	0.53	4.21	165.84
India (IN)	0	1.27	60.65
Japan (JP)	0	0	2.1
South Korea (KR)	0	0	0.05
Middle East (ME)	13.76	53.6	317.66
Rest of Asia (RA)	2.91	14.6	264.46
Russia (RU)	17.46	218.02	1,087.15
South Africa (SF)	0.28	7.58	37.95
South America (SM)	20.84	49.21	385.55
United States (US)	82.85	87.6	513.37
Eastern Europe (XE)	0.68	3.15	38.83

Note: Values in $GtCO_2$. Adapted from Gidden et al.[19].

Table 5 | Offshore regional triangular distribution parameters

Region	Minimum	Mode	Maximum
Africa (AF)	5.7	38.88	645.06
Australia & NZ (AU)	27.12	46.78	525
Brazil (BR)	20.2	27.09	211.71
Canada (CA)	5.25	34.73	368.66
China (CH)	2.91	20.02	72.73
Caspian Region (CP)	0	2.03	24.66
European Union (EU)	22.19	38.25	795.75
India (IN)	1.65	9.38	264.85
Japan (JP)	0.32	3.02	38.49
South Korea (KR)	0	2.31	19.96
Middle East (ME)	7.27	13.37	100.12
Rest of Asia (RA)	27.56	75.96	1,004.32
Russia (RU)	1.11	26.14	734.45
South Africa (SF)	3.86	5.45	42.72
South America (SM)	3.82	21.5	181.07
United States (US)	13.7	53.23	509.69
Eastern Europe (XE)	0.33	1.79	47.27

Note: Values in $GtCO_2$. Adapted from Gidden et al.[19].

Acknowledgments

The authors acknowledge the National Laboratory for Scientific Computing (LNCC/MCTI, Brazil) for providing HPC resources of the SDumont supercomputer, which have contributed to the research results reported within this paper.

A.S., and R.S. would like to acknowledge the Brazilian National Council for Scientific and Technological Development (CNPq) for the financial support. L.F.S., and L.B.B. were also financed in part by the Coordenação de Aperfeiçoamento de Pessoal de Nível Superior - Brasil (CAPES) - Finance Code 001.

Data and code availability

Selected datasets and codes of this study are hosted in a dedicated repository on Figshare (https://doi.org/10.6084/m9.figshare.00000000).

This repository contains python scripts utilized for statistical extraction data files and visualization of the data from this study. The provided datasets include regional and global statistical summaries for 1.5ºC and 2.0ºC ensembles, alongside with selected IPCC's AR6 C2 and C3 statistical summaries.

References

1. Intergovernmental Panel on Climate Change. *Climate Change 2022: Mitigation of Climate Change*. (Cambridge University Press, 2022).
2. UNFCC. *Conference of the Parties: Adoption of the Paris Agreement.* (Paris, France, 2015).
3. Schleussner, C.-F. *et al.* Overconfidence in climate overshoot. *Nature* **634**, 366–373 (2024).
4. Kazlou, Y. T., Cherp, A. & Jewell, J. Feasible deployment of carbon capture and storage and the requirements of climate targets. *Nat. Clim. Chang.* **14**, 1047–1055 (2024).
5. Riahi, K. & et al. Cost and attainability of meeting stringent climate targets without overshoot. *Nat. Clim. Chang.* **11**, 1063–1069 (2021).
6. Tavoni, M. *et al.* Implications of overshoot for climate mitigation strategies. *Nature Climate Change* Preprint at https://doi.org/10.1038/s41558-026-02563-7 (2026).
7. Warszawski, L. *et al.* All options, not silver bullets, needed to limit global warming to 1.5 ◦C: A scenario appraisal. *Environmental Research Letters* **16**, (2021).
8. Chiquier, S., Fajardy, M. & Dowell, N. Mac. CO2 removal and 1.5 °C: what, when, where, and how? *Energy Advances* 524–561 (2022) doi:10.1039/d2ya00108j.
9. Fuhrman, J. & et al. Rate and growth limits for carbon capture and storage. *Environmental Research Letters* **20**, 64034 (2025).
10. Lane, J., Greig, C. & Garnett, A. Uncertain storage prospects create a conundrum for carbon capture and storage ambitions. *Nat. Clim. Chang.* **11**, 925–936 (2021).
11. Smith, P. *et al.* Biophysical and economic limits to negative CO2 emissions. *Nature Climate Change* vol. 6 42–50 Preprint at https://doi.org/10.1038/nclimate2870 (2016).
12. Strefler, J. & et al. Between Scylla and Charybdis: delayed mitigation narrows the passage between large-scale CDR and high costs. *Environmental Research Letters* **13**, 44015 (2018).
13. Roe, S. *et al.* Land-based measures to mitigate climate change: Potential and feasibility by country. *Glob. Chang. Biol.* **27**, 6025–6058 (2021).
14. Fuss, S. & et al. Betting on negative emissions. *Nat. Clim. Chang.* **4**, 850–853 (2014).
15. Anderson, K. & et al. Controversies of carbon dioxide removal. *Nat. Rev. Earth Environ.* **4**, 808–814 (2023).
16. Smith, E. *et al.* The cost of CO2 transport and storage in global integrated assessment modeling. *International Journal of Greenhouse Gas Control* **109**, (2021).
17. Middleton, R. S. & Yaw, S. The cost of getting CCS wrong: uncertainty, infrastructure design and stranded CO_2. *International Journal of Greenhouse Gas Control* **70**, 1–11 (2018).

18. Streck, C. & et al. Considering durability in carbon dioxide removal strategies for climate change mitigation. *Climate Policy* **25**, 1–9 (2025).

19. Gidden, M. J. & et al. A prudent planetary limit for geologic carbon storage. *Nature* **645**, 124–132 (2025).

20. Grant, N. & et al. The policy implications of an uncertain carbon dioxide removal potential. *Joule* **5**, 2593–2605 (2021).

21. Weyant, J. Some contributions of integrated assessment models of global climate change. *Rev. Environ. Econ. Policy* **11**, 115–137 (2017).

22. van Beek, L., Hajer, M., Pelzer, P., van Vuuren, D. & Cassen, C. Anticipating futures through models: the rise of Integrated Assessment Modelling in the climate science-policy interface since 1970. *Global Environmental Change* **65**, (2020).

23. Cointe, B., Cassen, C. & Nadaï, A. Organising Policy-Relevant Knowledge for Climate Action: Integrated Assessment Modelling, the IPCC, and the Emergence of a Collective Expertise on Socioeconomic Emission Scenarios. *Science and Technology Studies XX(X)* **32**, (2019).

24. Tavoni, M. & Valente, G. Uncertainty in Integrated Assessment Modeling of Climate Change. *Perspectives on Science* **30**, 321–351 (2022).

25. Gambhir, A., Butnar, I., Li, P. H., Smith, P. & Strachan, N. A review of criticisms of integrated assessment models and proposed approaches to address these, through the lens of BECCs. *Energies (Basel).* **12**, (2019).

26. Cooke, R. M. Uncertainty analysis comes to integrated assessment models for climate change...and conversely. *Clim. Change* **117**, 467–479 (2013).

27. Bosetti, V. *et al.* Sensitivity to energy technology costs: A multi-model comparison analysis. *Energy Policy* **80**, 244–263 (2015).

28. Huard, D., Fyke, J., Capellán-Pérez, I., Matthews, H. D. & Partanen, A. I. Estimating the Likelihood of GHG Concentration Scenarios From Probabilistic Integrated Assessment Model Simulations. *Earths Future* **10**, (2022).

29. Marcucci, A., Panos, E., Kypreos, S. & Fragkos, P. Probabilistic assessment of realizing the 1.5 °C climate target. *Appl. Energy* **239**, 239–251 (2019).

30. Lontzek, T. S., Cai, Y., Judd, K. L. & Lenton, T. M. *Stochastic Integrated Assessment of Climate Tipping Points Calls for Strict Climate Policy*.

31. Gillingham, K. *et al. Modeling Uncertainty in Integrated Assessment of Climate Change: A Multi-Model Comparison*. http://globalchange.mit.edu/sponsors/all.Bosettiacknowledges (2018).

32. Guivarch, C. *et al.* Using large ensembles of climate change mitigation scenarios for robust insights. *Nature Climate Change* vol. 12 428–435 Preprint at https://doi.org/10.1038/s41558-022-01349-x (2022).

33. Beath, H. *et al.* A weighting framework to improve the use of emissions scenario ensembles of opportunity. *Nat. Clim. Chang.* https://doi.org/10.1038/s41558-026-02565-5 (2026) doi:10.1038/s41558-026-02565-5.

34. Calvin, K. *et al. IPCC, 2023: Climate Change 2023: Synthesis Report. Contribution of Working Groups I, II and III to the Sixth Assessment Report of the Intergovernmental Panel on Climate Change [Core Writing Team, H. Lee and J. Romero (Eds.)]. IPCC, Geneva, Switzerland.* https://www.ipcc.ch/report/ar6/syr/ (2023) doi:10.59327/IPCC/AR6-9789291691647.

35. International Institute for Applied Systems Analysis. AR6 Scenarios Database hosted by IIASA. Preprint at https://data.ece.iiasa.ac.at/ar6/ (2021).

36. Bastin, J.-F. *et al. The Global Tree Restoration Potential Downloaded From*. *Science* vol. 365 http://science.sciencemag.org/ (2019).

37. Griscom, B. W. *et al.* Natural climate solutions. *Proc. Natl. Acad. Sci. U. S. A.* **114**, 11645–11650 (2017).

38. Zanon-Zotin, M., Baptista, L. B., Rochedo, P. R. R., Szklo, A. & Schaeffer, R. Industrial sector pathways to a well-below 2 °C world: A global integrated assessment perspective. *Appl. Energy* **381**, (2025).

39. Müller-Casseres, E. & et al. International shipping in a world below 2^C. *Nat. Clim. Chang.* **14**, 600–607 (2024).

40. Kann, A. & Weyant, J. P. *Approaches for Performing Uncertainty Analysis in Large-Scale Energy/Economic Policy Models*. *Environmental Modeling and Assessment* vol. 5 (2000).

41. Kroese, D. P. *Monte Carlo Methods*. http://www.maths.uq.edu.au/ (2011).

42. Gentle, J. E., Hardle, Wolfgang. & Mori, Yuichi. Handbook of computational statistics : concepts and methods. in (2004).

43. Shields, M. D. & Zhang, J. The generalization of Latin hypercube sampling. *Reliab. Eng. Syst. Saf.* **148**, 96–108 (2016).

44. Riahi, K. & et al. The shared socioeconomic pathways and their energy, land use, and greenhouse gas emissions implications: an overview. *Global Environmental Change* **42**, 153–168 (2017).

45. Intergovernmental Panel on Climate Change (IPCC). *Climate Change 2021 – The Physical Science Basis*. *Climate Change 2021 – The Physical Science Basis* (Cambridge University Press, 2023). doi:10.1017/9781009157896.

46. Global Energy Monitor. Global Oil Infrastructure Tracker. Preprint at (2025).

47. World Bank. World Development Indicators (WDI) Database. Preprint at (2025).

48. International Energy Agency. IEA CCUS Database. Preprint at (2025).

49. Fuss, S. & et al. Negative emissions—Part 2: Costs, potentials and side effects. *Environmental Research Letters* **13**, 63002 (2018).

50. Popp, A. *et al.* Land-use futures in the shared socio-economic pathways. *Global Environmental Change* **42**, 331–345 (2017).

Supplementary Files

This is a list of supplementary files associated with this preprint. Click to download.

- SupplementaryInformation.docx